6th International Conference on "Latest Innovations in Science, Engineering and Management"
(IFUNA) Indian Federation of United Nations Associations, New Delhi (India) ICLISEM - 2017
12th November 2017, www.conferenceworld.in ISBN: 978-93-86171-76-4

"GROWTH OF CARBON NANOTUBES BY ARC DISCHARGE"

Upendra Sharan Gupta[1], Aadarsh S Chandran[2], Ayush Awasthi[3], Abhishek Pahwa[4]

[1]Reader Dept. of Mech .Engineering ,SVITS, Indore, (India)

[234]UGScholar Dept. of Mech. Engineering, SVITS, Indore, (India)

ABSTRACT

The mechanism of the SWNT synthesis in the arc discharge +processes appears to be fairly simple. It is governed mainly by the dynamics of hot vapor cooling and carbon diffusion through the bulk metal catalyst particle. It allows deliberate control of the arc processes and is the basis for the successful scaling-up efforts of the arc process. Semi quantitative treatment of the arc processes is possible. It provides a basis for a detailed mathematical modeling of arc reactors, which is necessary in order to design practical processes for maximum productivity, yield, and quality of SWNTs.

Scaling up the arc discharge processes of SWNT and MWNT production is possible and is realized in practice on an industrial scale. A production rate of 100 g/h of the raw product of each kind of these nanotubes is achieved per industrial apparatus. The economically reasonable limit for scaling up is already reached, but the challenge to further increase selectivity and specific productivity of the arc processes remains active.

Synthesis of SWNTs by the arc-discharge method is actually a CVD process that transforms amorphous carbon into a SWNT bundle with an appropriately large metal catalyst particle and proceeds in concordance with the DP kinetic mechanism.

Diffusion of carbon through the bulk metal catalyst particle is the rate-limiting step in all kinetically studied systems that grow long nanotubes. Therefore, in order to reach higher production rates, high-temperature processes should be developed, including CVD processes, ranging up to 1500°C, which appears to be the temperature limit for diffusion-controlled transition metal catalytic systems. For this development, the most difficult problem to resolve is to prevent thermal noncatalytic dehydrogenative condensation of the carbon source. In arc discharge synthesis of SWNTs, this problem is obviated by the use of amorphous carbon for the feedstock. Another important problem is the design of appropriate metal catalysts, which remains a poorly explored area.

Keywords: Arc Discharge method, SWNT,MWNT

 ISBN: 978-93-86171-76-4

I. INTRODUCTION

Carbon nanotubes produced from carbon vapor generated by arc discharge generally have fewer structural defects than those produced by other known techniques. This is due to the higher growth process temperature that ensures perfect annealing of defects in tubular graphene sheets. Multiwalled nanotubes (MWNTs) produced by these high-temperature methods are perfectly straight, in contrast to kinked tubes produced at low temperatures in metal-catalyzed chemical vapor deposition (CVD) processes. While the quality of low-temperature tubes can be improved by prolonged post synthesis annealing at temperatures above 2000 K, the mechanical and electrical properties of arc-produced MWNTs remain far superior. Very high-quality nanotubes are vital for many applications that do not require multi-ton tube quantities; therefore, high-temperature production methods will not be completely replaced by more productive catalytic methods. On the contrary, the need of industry for the highest quality nanotubes will likely steadily grow, thus making it necessary to scale up the high-temperature production methods. Single-wall nanotubes (SWNTs) are almost lacking in structural defects independent of the synthesis process; therefore, alternative methods already strongly compete with arc technique and may surpass and substitute for them in future bulk production. The extent of this substitution will depend on other important qualities of the SWNT product, such as uniformity of tube chirality, size distribution, and ease of purification. Thus, there are grounds to intensively pursue both further studies and methods of scaling up each process. Knowledge of the nanotube growth mechanism is the basis for success in scaling up efforts and in obtaining desirable nanotube qualities, and therefore it must be given much attention.

At present, the arc method remains the easiest and cheapest way to obtain significant quantities of SWNTs, but the as-produced nanotubes are less pure than those produced by other modern methods. Hence, many experimental and theoretical studies attempt to improve the SWNT yield in the arc process and to provide a comprehensive understanding of the growth mechanism. Scaling up, optimizing, and controlling the arc process to make it commercially viable is an important challenge.

II. ARC DISCHARGE PRODUCTION OF MWNTS

2.1 General Technical Features of the Production Process

The carbon arc technique for generating MWNTs appears very simple, but obtaining high yields of tubes is difficult and requires careful control of experimental conditions. In the most common laboratory scale production scheme, the direct current (DC) arc operates in a 1- to 4-mm wide gap between two graphite electrodes 6 to 12 mm in diameter that are vertically or horizontally installed in a water-cooled chamber filled with helium gas at sub atmospheric pressure. Helium gas and DC current are more important to maximize yield; the position of the electrode axis does not noticeably affect the MWNT quality or quantity. The 50- to 250-mm long positive electrode (anode) is consumed in the arc, whereas a cylindrically shaped cathode deposit (boule, or slag) is grown on the negative electrode. The linear growth rate of the deposit along the electrode axis is smaller than the rate of anode consumption, so one of the electrodes is advanced automatically into the arc zone with a feed rate (FR) of about 0.5 to 3 mm/min to prevent gap growth. The most stable and high yield arc process

requires a constant feed rate and arc current for the duration of synthesis [1]. Under these conditions the arc gap and the voltage drop across the gap remain constant, ensuring constant arc power. In this regime, the voltage measured on the electrode that leads outside the chamber grows during the run because the resistance of the anode graphite rod decreases faster than the resistance from the cathode deposit increases. This total voltage change does not alter the properties of the arc plasma and thus the nanotube yield.

The holders for the graphite cathode and anode rods are usually water-cooled to prevent damage that might otherwise occur when the arc is near either the cathode or the anode holder. The cooling affects the properties of the cathode deposit only a few millimeters from its origin; the rest of the deposit up to 10 to 15 cm total length has a consistent cross-sectional structure and composition. During those first few millimeters (up to 1 cm) of the cathode deposit growth, the arc process stabilizes and a steady electrode surface temperature is developed. Subsequently, the cooling of the cathode no longer influences the deposit working surface temperature. Therefore, it is expedient to use a cathode of sufficiently small diameter (i.e., equal to or smaller than the anode rod diameter) that is long enough (i.e., a few centimeters) to more quickly attain a steady temperature at the cathode working surface and in the arc. Furthermore, the cathode deposit is more strongly attached to a smaller diameter cathode than to a larger one. A strong bond is important to prevent the cathode deposit from breaking off of the cathode surface in the course of the production process. This cleavage happens most frequently with long cathode deposits, horizontal electrodes, and vigorous arcs. Accordingly, excessive cooling of the cathode holder is undesirable. The same is true for the anode holder. When the arc zone approaches to within 1 to 2 cm of the cold anode holder, the anode working surface becomes cooler, which alters the plasma properties, thus deteriorating the uniformity of the deposit structure and composition. Low-heat conductive anode holders are therefore equally advisable.

The helium gas atmosphere can be static or dynamic during the process with no difference in product quality observed. The requirements for helium gas purity are much less rigid than for fullerene or SWNT synthesis; 99.5% and 99.999% pure gases produce equivalent MWNTs. The MWNT synthesis is much more tolerant to the presence of oxygen-containing impurities in the buffer gas, because MWNTs are formed in the interelectrode gap, where the gas does not penetrate, whereas fullerenes and SWNTs are formed well outside the gap.

2.2. Composition and Structure of Cathode Deposit

The internal structure of the deposit provides the most insight into the MWNT growth process in the arc. Improved understanding of the mechanism of MWNT growth in the arc is essentially based on the comparison of arccharacteristics with deposit structure studied initially by scanning electron microscopy (SEM) and transmission electron microscopy (TEM).

Individual MWNTs were first found on the cathode surface by Iijima [2]. Soon after this discovery, Ebbesen and Ajayan found conditions for producing large cylindrical cathode deposits containing gram quantities of MWNTs [3,4]. Such cylindrical deposits consist of a hard gray outer shell, typically about 1.5-mm thick, and a soft fibrous black core. The shape of the deposit cross section closely mimics that of the consumed anode. For example, an anode rod with a square cross section produces a cathode deposit with a similar cross section and a

squared core.TEM analysis identified three distinct structural components within the core material obtained under near-optimal conditions: MWNTs in the amount of approximately 35 wt %, multiwall polyhedral particles (MPPs, ca. 45%), and various kinds of graphitic particles (ca. 25%). Along with tubes and MPPs of approximately isometric shape, various intermediateparticle shapes are observed in small quantities, e.g., elongated particles constructed of several fused multilayer cones. Graphitic particles have been mainly found as curved ribbons made of stacked graphene layers. Relative amounts of these components, as well as nanotube and MPPs size, as assessed by TEM observations, strongly depend on the arc parameters as illustrated in Table 3.1. Core material produced at low helium pressure contains a small amount of tubes, and thus the main component of specimen 1 was curved graphite. The tendencies for the tube yield to increase and for the graphitic particles to decrease with an increase in He pressure and a decrease in arc current are clearly revealed by the first three examples in Table 3.1. This is further confirmed by studies performed at higher-than-atmospheric He pressures. Thus, in specimen 6, the main components were nanotubes and MPPs. The range of nanotube and MPP diameters observed at higher pressures is much wider than at low pressures. However, it should be noted that the most probable diameter of MWNTs does not change much with conditions and is about 14 nm. Lower feed rates and thus wider gaps also lead to broader size distributions.

Table 1 Parameters of the MWNT Arc Synthesis with 6-mm Diameter Anode Rods

N	He, Torr	I, A	Feed Rate, mm/min	Gap Width, mm	Voltage Across the Gap, V	Deposit Diameter, mm	Deposit Growth Rate, mg/min	MWNT Amount, %	MWNT Diameter, nm	MPP Amount, %	MPP Diameter, nm	Graphitic Particles, %	Fullerene Yield in Soot, %
1	100	80	4	3.9	18.0	7.8	115	5	8–20	25	—	70	17.9
2	200	65	4	2.2	19.0	6.5	170	10	8–22	40	20–85	50	18.0
3	700	55	4	0.5	20.8	7.4	260	20	8–23	45	20–90	35	5.5
4	500	65	8	0.4	21.3	8.0	350	20	5–29	30	19–93	50	5.8
5	500	65	2.5	3.5	22.3	7.6	90	30	5–46	60	9–93	10	14.3
6	1500	65	1.4	4.2	31.1	5.5	20	35	4–60	40	8–120	25	20.1
7	2000	65	1.4	3.3	32.1	5.5	22	30	4–60	40	8–120	30	20.3
8[a]	500	160	0.65	0.8	22.4	11.6	160	30	5–50	45	10–90	25	12.6
9[b]	500	132	1.0	1.7	22.2	10.9	195	30	5–50	40	15–80	30	10.1

Note: N.A. Kiselev et al. Carbon 37, 1093 (1999). With Permission.
[a] Anode rod diameter 10.6 mm.
[b] Rod 9.8 mm.

No sole externally controlled parameter may be identified as the crucial factor for deposit component distribution. Comparable yields of MWNTs can be obtained with narrow and wide gaps. Composition and structure of a deposit is dependent on carbon vapor properties inside the gap, such as the pressure and temperature distribution, the presence and mobility of carbon particulates, and the dynamics of graphite vaporization and carbon vapor condensation. These are determined by a multitude of externally controlled factors, including He pressure, arc power, graphite anode qualities, and the arc experiment geometry.

SEM studies of the samples prepared in a way that does not disturb the intrinsic structure of the core components have produced the following data and concepts [1]. The hemispherical caps of the columns are densely covered with nanotubes that lay along the surface or at angles exceeding 45° from the column axis. Some tubes protrude from the upper layer into the free space, thus leading to the possibility of using a separated column as a small electron field emitter cathode. When embedded in the core, the columns serve as leads for electron current to the cathode surface and column tops as a principal place for emitting electrons into plasma

[5]. The highest concentration of nanotubes is found in low-density intercolumnar spaces (denoted as zone 2, with the column itself as zone 1 in [5]) and on the side surface of a column. SEM examination of a cross-sectioned, separate column reveals an area of enhanced emission of secondary electrons along its circumference, thus supporting this observation. This circumferential area is composed of interlaced nanotubes forming an outer braid to the column. This braid is generally several microns thick, with no significant inclusions of MPPs or graphitic particles. The tubes in the braid are oriented preferentially normal to the tube axis, with statistically reliable observations showing that more than 50% of nanotubes are inclined at angles exceeding 45° relative to the deposit axis. The same is true of nanotubes in zone 2. The inner part of a column inside the braid consists of a disordered mixture of graphite-like particles, MPPs, and a small number of nanotubes.

2.3. Growth Mechanism

From the mode of nanotube and other component packing in the core described above, some refinement of the model [5] offered to describe the growth of the deposit in a direct current arc seems necessary [1]. In this model the tips of parallel nanotubes in zone 1 (column top) act as field emitters of electrons into the plasma. This electron injection produces a high degree of carbon ionization resulting in con-centration of carbon ion current flow above the columns. This flow provides the principal feedstock for column growth. The helium buffer gas is drawn in by the carbon ion flux to the top of the columns, is swept to the side, and then returns back to the plasma over zone 2, which is the intermediate area between adjacent columns. The refinement of this model is as follows and is illustrated by Figure 1. In the absence of a large amount of vertically oriented nanotubes, the emission of electrons from zone 1 is likely to be mainly thermionic in nature and occurs from a variety of constituents of the columns. The dominating abundance of horizontally packed nanotubes over the column top surface probably indicates that that the electric field effect at the open end of a nanotube is not a governing factor for its growth. Those nanotubes that were originally located near the very hot top of a hemisphere could then undergo evaporation, yielding neutral carbon particles. An estimate has shown [5] that the majority of carbon precipitated on columns must evaporate back as neutrals. Evaporation enriches the central part of a column in MPPs and graphitic particles to the extent eventually observed with the SEM, as these non-tube components are thermodynamically more stable than nanotubes [19]. Another reason for the enrichment of the central part of a column with graphitic particles is that they probably carry large positive charges while moving toward the cathode [20] and are strongly attracted by the negatively charged volume over the column top. Helium transports re-evaporated neutral carbon molecules to zone 2, where they serve as a principal feedstock for the growth of new nanotubes [5].

Carbon is vaporized from the porous surface layer of a polycrystalline graphite anode mainly in the form of graphite crystallites exceeding 3 nm in linear size. Small crystallites serve as the main positive charge carrier in the carbon plasma, as their work function is much lower than the ionization potential of small carbon molecules, which are the minor carbon ingredient. Crystallites undergo vaporization on the way to the cathode, generating small carbon clusters (mainly C3) and diminishing in size. It takes about 1 ms for carbon species to cross a few millimeters wide arc gap, and during this time the smaller crystallites are fully vaporized, whereas larger

crystallites reach the cathode surface and thus are present in the deposit. Structural peculiarities of the graphitic particles found in the deposit may be brought about by delamination of original crystallites and other thermal transformation processes. On the average, the deposit material is enriched in isotope 12C relative to the graphite anode [21]. Graphitic particles thus formed cannot contribute to the shift in isotope distribution, leaving MWNTs and MPPs solely responsible for the shift observed. This strongly suggests that the MWNTs and MPPs have been built from the low-molecular carbon species, mainly from C3, C2, and C1 carbon clusters.

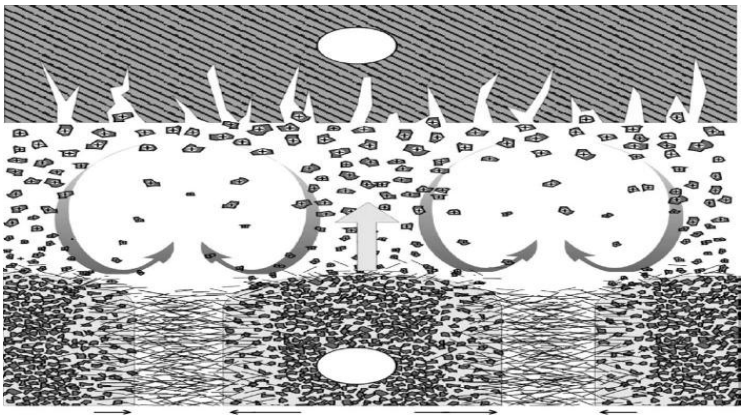

FIGURE 1 Schematic of MWNT growth in a DC arc. Positively charged graphitic splinters spallated from the anode partially vaporize on the way to the tops of the columns (zone 1). Intense carbon flux above the columns is due to enhanced thermionic emission from zone 1, which produces a high degree of carbon vapor ionization. Carbon density above the columns is further increased by circular convection of helium. Nanotubes grow in dense gas near the cathode surface from low-molecular carbon species and precipitate in zone 1 and zone 2 with their axes oriented preferentially parallel to the surface. This orientation is held constant in as-produced deposit core in both zone 2 and the nanotube braid of the column [1].

In the vicinity of the cathode surface, a relatively high carbon-vapor density is built up because the carbon hitting the ca. 3200°C [8] hot surface cannot be totally accommodated in the solid, and thus low-molecular-weight carbon clusters are easily re-evaporated [5,9,23]. The MWNTs are self-assembled from small carbon clusters in this gas layer and then migrate to the cathode surface with the flux of charged and neutral carbon particles and deposit on it preferentially parallel to the surface, an orientation that ensures stronger adhesion of tubes to core components. An adequately high carbon-vapor density in the layer is critical for tube self-assembly to occur [9,24]. Below a certain threshold value of vapor density, the MWNTs are not able to self-assemble, and the only mode of carbon vapor deposition then is formation of two-dimensional graphene structures on vapor-exposed surfaces, which generally takes place in the deposit shell region. This vapor density threshold is very narrow, as indicated by the commonly observed very sharp transition between the core and the shell structures and by independent orientation of the core columns and the shell layers. This transition occurs at around 2000°C, which is the temperature of the inner surface of the shell [9]. The necessity of sufficiently high carbon

vapor pressure for MWNT growth was established also in experiments using laser evaporation of graphite. They have shown that the yield of MWNTs increases with better concentration of the laser beam, and that synthesis is possible only with the reaction chamber temperature elevated to at least 1200°C [24]. In the arc under conditions of low anode evaporation rate, the yield of MWNTs also falls drastically [9]. Finding MWNTs embedded in the fullerene containing soot deposited on chamber walls further emphasizes that they are self-assembled in the gas phase. Although usually very rare, such occasions become more common with very wide gaps when the narrow gas layer adjacent to the cathode is more efficiently swept into the chamber volume. Installing an additional negatively biased electrode near the gap also facilitates extraction of MWNTs from the gap [25].

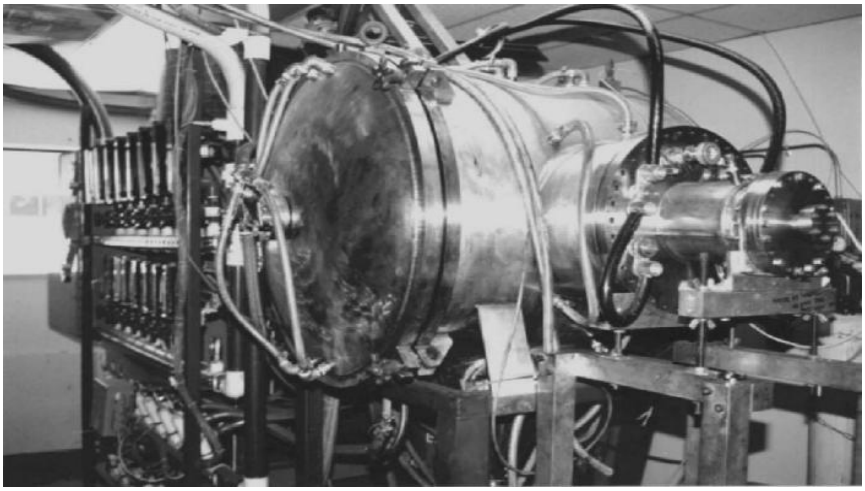

Figure 2 Industrial arc-discharge reactor for producing fullerenes and carbon nanotubes. Features vaporization of up to 1 kg of anode per hour [26].

The nanotube-rich columnar deposit formation is a steady-state realization of a nonlinear multi-parameter kinetic process. Therefore, the nanotube growth optimization strategy should address the following factors. All the parameters of the arc process are interdependent, and an attempt to adjust only one of them will lead to inevitable variation of others. Different sets of externally controllable parameters can give similar tube content. It is not productive to optimize tube growth under conditions of unstable arc operation, and it is of prime importance to first identify the stable regions among the set of possible experimental parameters. The conditions listed in Table 1 illustrate only a few, though important, stable solutions to the problem of optimal nanotube production [1]. However, variations in materials and equipment may necessitate adjustments of the given conditions to obtain reproducible results.

2.4.Scaled-Up MWNT Production Process

A further increase in MWNT production rate was expected by employing thicker graphite rods in larger, more powerful arc reactors. This expectation was realized with the construction of a large-scale arc reactor with a 350 L chamber capable of vaporizing up to 75-mm diameter graphite rods [26]. The cylindrical cathode deposits obtained with this scaled-up process contain soft core within the outer hard shell. Under optimized conditions the core material has the columnar structure. The column diameter and separation are about the same as in small-diameter deposits. The column length in large deposits is commonly much lower (ca. 3 to 5 mm) because of lower plasma stability in the arc gap. Optimal conditions for MWNT production occur in the same range of helium pressure and arc gap widths but at substantially lower current densities compared with laboratory-scale anodes. More efficient thermal insulation of the inner part of the electrodes by the outer shell layer is responsible for lower energy requirements for vaporizing the anode and maintaining sufficiently high temperature and carbon vapor density over the core region. This insulation also results in a more concave cathode growth surface and more convex anode erosion surface than in laboratory scale electrodes. With such gap geometry, a steeper radial fall of temperature and carbon vapor density takes place, resulting in a less-even radial distribution of deposit core components compared with thin electrodes. Nevertheless, the average amount of MWNTs in the core is similar to that in thin cathode deposits, although under the current best conditions it is still 20 to 30% lower. Further optimization of the large-scale process is likely to reduce or eliminate this difference, as no principal limitations have been revealed. At present, the kilogram per run productivity of the large-scale process compensates economically for the somewhat lower MWNT content of the product. The concomitantly reduced cost of arc-derived product stimulates its use in applications that require MWNTs of the highest structural quality. The Young's modulus of MWNTs is calculated to be ca. 1000 to 1500 GPa and has been measured at 1000 to 3700 GPa. The measured tensile strength is 11 to 63 GPa for the MWNT outer layer. The thermal conductivity along the length of the tube is ca. 1500 W/m K, and the resistivity is ca. 0.1 □ □cm. The market niche for arc-produced MWNTs will persist until a method of producing better quality MWNTs appears.

A further increase in vaporized rod diameter and in arc power is technically feasible but does not appear to be economically justified [26]. The large-scale reactor described above has been demonstrated to be close to the optimum size and power for MWNT synthesis in the arc and will probably remain the largest reactor in the world for years to come. In the arc process, the next logical step for increasing MWNT output will be automation of large-scale reactors, which will render the production process nearly continuous.

III. PRODUCTION OF SWNT$_S$

SWNTs are produced in an arc process utilizing co-vaporization of graphite and metal in a composite anode [30,31] commonly made by drilling an axial hole in the graphite rod and densely packing it with a mixture of metal and graphite powders. Various pure elements and mixtures have been used to fill the rod, including Fe, Co, Ni, Cr, Mn, Cu, Pd, Pt, Ag, W, Ti, Hf, La, Ce, Pr, Nd, Tb, Dy, Ho, Er, Y, Lu, Gd, Li, B, Si, S, Se, Zn, Sn,

Te, Bi, Cd, Ge, Sb, Pb, Al, In, Fe/Co, Fe/Ni, Fe/Co/Ni, Co/Ni, Co/Pt, Co/Cu, Co/ Bi, Co/Pb, Co/Ru, Co/Y, Ni/Y, Ni/La, Ni/Lu, Ni/B, Ni/Mg, Ni/Cu, Ni/Ti [32–46], but at present only Ni/ Y and Co/Ni catalysts are commonly used in SWNT production.

These preferred systems share many common features. Both perform better in helium atmosphere than in argon, at about 0.6 bar pressure. The process is most efficient with a stable arc discharge and a constant anode erosion rate, corresponding to ca. 2 A/mm^2 current density and ca. 3-mm gap width. This is better achieved by maintaining a constant arc current and anode feed rate and thus constant arc gap width.

A cylindrical deposit grows at the surface of the cathode. The weight of the deposit constitutes about one half of the weight of the anode consumed in the process. The deposit consists of a hard-gray shell and a soft core. The core has poorly developed columnar structure and contains MWNTs, MPPs, and graphitic particles. In the Co/Ni system, commonly operating with ca. 2 at% metals in the anode, the core is diamagnetic and does not contain any metal components. High temperature prevents precipitation of metal vapor on the growth surface, and all metal escapes the gap. However, the outermost layer of the gray shell contains trace amounts of metals, introduced by gas convection onto the exposed side surface. In many other systems, especially with high metal loading of the anode, the deposit may contain metal-filled MWNTs and MPPs or bare spherical metallic particles [47]. In the Ni/Y system the deposit contains large amounts of yttrium [48], whereas metal nanoparticles found in the chamber are enriched in nickel [46,48,49].

The mixed carbon and metal vapor, which has escaped the gap, then condenses into the product, which moves to the reactor surfaces and deposits on them. The product is divided into three distinct structural types, depending on the deposition area. A spongy soft belt called *collaret* is formed around the cylindrical deposit and represents about 20% of the product weight. Relatively strong clothlike soot on the chamber walls represents another 70%, and the remaining 10% of the product is a weblike structure suspended in the chamber volume between cathode and walls. All three types contain varying amount of SWNTs, fullerenes, amorphous carbon, empty and metal-filled MPPs, *naked* metal particles, and graphitic nano and micro-particles. Thermogravimetric analysis (TGA) and near-infrared (NIR) spectroscopy [50] are used to accurately determine the metal and SWNT content in the arc material, whereas electron microscopy (TEM and SEM) and Raman spectroscopy (RS) generally provide only rough assessments of the concentration of product components. These methods appear to be the most useful for analyzing arc-product composition and structure. The collaret contains more SWNTs and metal particles than other components of the product. This difference is about 20% for Co/Ni and 50% for Ni/Y systems. The collaret is formed from an electrostatically deflected flow of soot that is propagating away from the gap. SWNT growth continues in the material that is deflected and captured on the deposit surface for a longer time, leading to enrichment of the collaret in SWNTs. The SWNT yield averaged among all three structural types of the product is about the same in these systems, roughly ca. 20 □ 5% of the total product weight. Fullerenes C_{60} and C_{70} contribute ca. 5 to 10 wt% to the total product weight in the Co/Ni system and ca. 1% in the Ni/Y system. The average mass fraction of the metal catalyst is ca. 20% of the total product weight in the Co/Ni system and 35% in the Ni/Y system. Amorphous carbon constitutes ca. 50 wt% of the total product weight and graphitic particles ca. 5 wt% in both cases.

3.1. Metal Catalyst Particles

The efficiency of SWNT synthesis in a carbon/metal arc is determined primarily by the choice of metal catalyst for the process. It was found [33,34] that catalysts composed of two metals produce much higher yields of SWNTs than did individual metals. The ratio of metals in the original catalyst mixture also produces a drastic effect on SWNT yield. In the Co/Ni catalyst arc system the highest yield is obtained with Co:Ni = 3:1 ratio in the original mixture . For the Ni/Y catalyst the optimum molar ratio of the original mixture was determined to be Ni:Y = 4.2:1 [46]. The predominant diameter of metal particles in the arc SWNT product is 10 to 30 nm, and the metal ratio in these particles differs from thatin the original metal mixture. The energy dispersive x-ray fluorescence (EDX) analysis has shown that the metal composition of different particles varies within 30% from the 3:1 ratio of cobalt to nickel in the original mixture [61]. The same-size metal catalyst particles in the Ni/Y system are essentially depleted of yttrium [46,49], regardless of the Ni:Y composition of the original catalyst mixture [49]. This implies that there are additional functions for yttrium in the arc synthesis, besides forming catalytic particles of the optimum composition. The presence of yttrium may facilitate an adjustment of the optimal process temperature through the highly exothermic reaction of yttrium carbide formation. This reaction brings about higher catalytic particle temperature, which results in a generally observed 0.1- to 0.2-nm shift to larger average tube diameter, compared to that produced with yttrium-free catalysts under otherwise similar conditions. The 3Co/Ni mixture produces only long SWNT bundles with 1.2- to 1.3-nm diameter nanotubes. The Ni/Y system, in addition to long bundles, under certain conditions can generate [49] short bundles (~ 50 nm in length) composed of thicker SWNTs, with an average nanotube diameter of 1.8 nm, radiating from metal catalyst particles (sea urchin structures). Long bundles of narrow tubes generally grow from particles containing less yttrium (below 15%) than metal particles in sea urchin structures (over 11% yttrium) [49]. These facts may imply that sea urchin structure tubes grow from hotter metal particles and that the presence of yttrium in the metal particle retards the start of tube growth until a higher carbon supersaturation is attained than for a pure nickel particle. As a result, sea urchin tube growth starts simultaneously over the whole metal particle surface. The sea urchin metal particle cools down very quickly to temperatures at which dissolution of carbon becomes too slow to sustain steady tube growth. In addition, the bundle roots covering the whole metal surface prevent the outside carbon feedstock from coming in contact with the metal particle surface. When the carbon inside the particle is exhausted, growth is terminated, resulting in short bundles. The amount of carbon in these bundles is commensurate with that dissolved in the metal particle at the start of growth.

3.2. Dynamics of SWNT Growth in the Arc Process

Carbon vapor flowing from a sufficiently narrow arc gap can be idealized as a turbulent jet of cylindrical symmetry [22,62] and described in the framework of a semiempirical theory [63] of heat and mass transfer in a free turbulent jet. These transfer phenomena control the dynamics of carbon vapor mixing with helium gas and the resulting cooling. In the framework of the turbulent jet model, an analytical relationship between the essential parameters of the arc process is valid [22]. These parameters includethe volume rate of carbon vapor

flow from the gap V_{soot}, the carbon vapor temperature T_o and velocity $U_o$at the cylindrical boundary of the gap, the helium pressure in the reactor P, the gap width $h_o$andelectrode diameter $2r_o$, and the characteristic time for turbulent mixing and cooling of carbon vapor τ_{mix}.The value of τ_{mix} is connected to other parameters by Equation (3.1):

$$\tau_{mix} = r_o^{1.5}/U_o h_o^{0.5} = 2\pi r_o^{2.5} h_o^{0.5} P/V_{soot} R T_o$$

The rate of carbon vapor cooling in a turbulent jet outside the gap is directly proportional to the linearrate of carbon vapor propagation U_o and thus to the volume rate of vapor generation V_{soot} and to the inverse value of the chamber pressure P. Temperature T_o can be either determined experimentally orevaluated under the assumption that the equilibrium carbon/metal vapor pressure in the gap is equal to the ambient gas pressure in the chamber. The volume of carbon/metal vapor produced should allow for vapor composition. It should be noted that the true value of the cooling rate in a real arc system may differ from that calculated with Equation (3.1), because the model considers only turbulent cooling and because of uncertainties in the values of the parameters involved. In this respect, it is noteworthy that laminar diffusion of cold environment helium into the hot zone, which also includes the gap area, can substantially contribute to the rate of reagent cooling [22]. This contribution becomes stronger with wide gaps [22]. However, the laminar diffusion cooling rate has similar pressure and temperature dependence to that of the turbulent case, so in the first approximation this should change only the proportion between the characteristic cooling time and the other process parameters in Equation (3.1), without disturbing the underlying dependence. Assessments show that τ_{mix} value, as determined by Equation (3.1) functional dependence, can be treated as having an accuracy better than a factor of 3 in the analysis of arc synthesis performance in the whole range of arc process conditions.The parametric study of SWNT yield in the 3Co/Ni arc system was performed in a wide range of helium pressures, arc currents, and FRs, and the data were evaluated in relation to the turbulent jet model. The gap width and rate of vapor generation were measured in each run, and vapor temperature inside the gap was assessed as previously to calculate the □$_{mix}$ value.

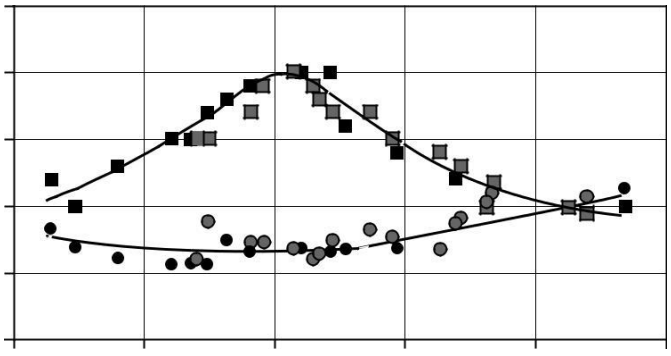

Figure 3 Dependence of the yields of SWNTs (squares) and fullerenes (circles) on the characteristic time ofturbulent mixing of the hot carbon vapor with helium gas in the fan jet flow moving from the interelectrode gap. Data points correspond to a wide variation of externally controlled arc discharge process parameters (helium pressure, arc current, and electrode feed rate) [61].

The dependence of the SWNT yield on the τ_{mix} value is presented on figure 3. All SWNT yield data points are grouped around a common curve peaking at ca. 6 ms. This means that τ_{mix} is the sole parameter determining the yield of SWNTs. The largest SWNT yields occurring near τ_{mix} = 6 ms correspond to fairly different sets of helium pressures, arc currents, and gap widths. This implies that no unique set ofexternally controlled parameters exists that would produce the highest SWNT yield for a given system. The parameter to optimize the process for the highest SWNT yield is τ_{mix}. SWNT production in the arcprocess is totally controlled by the cooling rate of carbon vapor escaped from the gap, and formation of nanotubes occurs at a distance of a few centimeters from the arc gap. The cooling time τ_{mix} = 6 ms, which is optimal for SWNT production, gives characteristic time of the SWNT growth process. Assuming 20 μm as the average SWNT length, the linear growth rate of SWNTs is ca. 3 mm/s. This value is many orders of magnitude higher than the linear growth rate of MWNTs formed on metal catalyst particles at lower temperatures, which implies that diffusion of carbon through the metal particle is the rate limiting step in catalytic nanotube growth.

3.3. Carbon "Dissolution-Precipitation" Model

The carbon "dissolution-precipitation" (DP) kinetic model developed a long time ago for the growth of carbon filaments and MWNTs on bulk metal nanoparticles [66–69] was subsequently adapted with some modifications for SWNT growth from similarly massive catalytic nanoparticles in the arc discharge and [49, 51,70–74]. The model includes three consecutive steps: dissolution of carbon coming into contact with the bare metal surface, transfer of dissolved carbon to another location on the particle surface, and precipitation of carbon as nanotubes at this location. Dissolution of amorphous carbon into metals of the iron group is a highly exothermic process. It keeps the particle hot enough to produce SWNTs in the tube formation zone a few centimeters away from the arc, where otherwise the particle temperature would be too low. The round shape of particles found in the product attests to their molten state during the process. Particle melting is facilitated by the incorporation of carbon into metal. The temperature of the carbon-containing, molten catalytic particle in the SWNT synthesis zone is assumed to be near 1300°C, the eutectic temperature of the metal-carbon mixture [49,51,75,76]. Carbon solubility in the particle at SWNT synthesis temperature can be estimated as 2 to 3 wt%, using the binary M-C phase diagrams of cobalt and nickel. Small supersaturated catalytic particles may contain up to four times as much carbon [75,77].

Carbon diffusion through the catalytic metal particle has been shown to be the rate-limiting stage of the overall DP process in the case of vapor-grown carbon fiber (VGCF) and MWNT synthesis by catalytic pyrolysis of hydrocarbons [66–69]. In the framework of the DP model, the rate of SWNT growth can be estimated for arc synthesis as well. The carbon diffusion flux through the catalytic nickel particle at 1300°C can be evaluated as $Q = D \cdot \text{grad } C \sim 2 \cdot 10^{-6}$ cm^2/s $\cdot$ 1 $\cdot$ 10^5 g/cm^4 ~ 0.2 g/cm^{2}s. The carbon diffusivity of $2 \cdot 10^{-6}$ cm^2/s was obtained from the temperature dependence $D = 0.1 \exp(-140 \text{ kJ} \cdot \text{mol}^{-1}/RT)$ for nickel [78]. The carbon concentration gradient 1 $\cdot$ 10^{5}g/cm^{4}was estimated using the assumptionthat carbon concentration at the dissolution spot exceeds that at the precipitation spot by ~0.2 g/cm^3, which is about the value of carbon solubility, and the distance between these spots is 20 nm. Division of carbon flux value 0.2 g/cm^2 s by the

gravimetric density of the SWNT bundle (~ 1 g/cm^3) yields 0.2 cm/s for the value of the SWNT linear growth rate. This value (0.2 cm/s) practically coincides with the value for SWNT linear growth rate of 3 mm/s independently. This coincidence implies that carbon diffusion through the catalyst nanoparticle is the limiting stage of the overall SWNT production process.Given the carbon flux of ~0.2 g/cm^2 s through the typical size 20-nm particle, and the characteristic SWNT growth time of 6 ms, it is easy to calculate that the fraction of particles active in SWNT production should be only about 1% of the total particles. This is close to what is observed by TEM in the arc synthesis products.

Carbon atoms, brought by diffusion from inside the liquid particle to the surface, start to arrange into a small carbon network containing a few hexagons and pentagons. When this network grows to the diameter of a nanotube and incorporates six pentagons, it has a more or less hemispherical structure with carbon atoms on the circumference of the hemisphere chemically bonded to the surface atoms, which can be either metal or carbon atoms. Other carbon atoms of the hemisphere form a carbon network peeled away from the surface. This scenario is very close to the construction of a SWNT cap by a computer through the molecular dynamics modeling of the segregation of carbon from hot metal-carbon alloy[49] The SWNT cap diameter is energetically "locked up" at this point, and further addition of carbon atoms to the hemisphere root result only in formation of hexagons in the wall of the growing SWNT, independent of slight changes of synthesis conditions at the root area.

At a higher temperature, a larger number of hexagons are included in the hemisphere structure together with the six pentagons, because the more intense supply of carbon atoms reduces the probability of pentagon formation. Thicker SWNTs therefore emerge at higher temperatures.

Growth of all SWNTs in a bundle starts simultaneously [49] from an active spot on the particle surface. The local temperature of multiple SWNT nucleation sites belonging to an active spot does not vary much, and therefore one-spot bundles consist of nanotubes that are very close in diameter [46,60,79,80] with a strong tendency to contain tubes of uniform chirality [60,79,80]. Several small neighboring spots can coalesce, giving rise to a combined bundle composed of discernible narrow bundles [46,73]. For a substantial portion of their length, bundles originating from different particles can also combine into a thick bundle while drifting in the gas phase or during ultrasonic treatment of the SWNT product in a liquid. Combined bundles of both types can contain SWNTs of substantially different diameters and chiralities [81–88].

The above-proposed molecular model for nanotube growth from a molten metal/carbon particle explains origin of the preferred chirality in tubes. Insertion of carbon atoms into the M-C bonds at the nanotube root cannot proceed without the relative displacement of metal atoms tangentially along the tube circumference, when the tube is chiral. With achiral tubes this displacement can be smaller, or negligible for armchair tubes with a certain type of M-C coordination bonding. For a larger helical pitch of chiral tubes this displacement is larger. The displacement should generate torque that will cause mutual rotation of the tube and the ensemble of metal atoms bound to the tube root, about the tube axis. The rotation will be hindered because of the high viscosity of molten metal and van der Waals interactions among the tubes in the bundle. At a certain bundle lengths the van der Waals retardation of tube rotation prevails over circular metal ensemble drag friction, and mutual rotation of

tubes in the bundle will cease. Activation energy of circular metal ensemble motion in the surrounding liquid can exceed or even far surpass that of achiral (armchair) tube growth, thus slowing down or preventing further growth of chiral tubes. As a result, the armchair tubes grow in preference to zigzag and chiral tubes, especially to those chiral tubes that have large helical pitch. This preference has been observed in many studies and is commonly attributed to higher thermodynamic stability of the armchair tubes, particularly the (10,10) tube. The kinetic mechanism for tube chirality selection outlined above finds support in several observations. The core of a bundle is likely composed of only armchair tubes, whereas the outer shell of a bundle consists of chiral tubes [79–88]. This is expected with the kinetic mechanism, as outer tubes in the bundle have more opportunities for rotation due to weakened van der Waals interactions. Also anticipated is more frequent occurrence of nonzero chirality in tubes that are seen lying apart from bundles [79–88], as these tubes most likely have been individually grown or detached from the outer layer of a bundle during sample preparation. In either case, nonzero chirality is presumed by the kinetic selection mechanism. It also predicts that a higher metal particle temperature would favor formation of chiral tubes and larger helical pitch, whereas lower temperature should facilitate armchair tube dominance in the product.

3.4. Scaled-Up SWNT Production Process

The dynamic model of the carbon arc implies no principal limitations for obtaining high SWNT yields with much larger-diameter graphite/metal anodes than are commonly used in laboratory scale practice. In essence, it predicts that a high SWNT yield would be retained if the value of characteristic cooling time τ_{mix} is maintained at ca. 6 ms while using a larger rod diameter $2r_o$. According to expression (1) for τ_{mix}, to compensate for the growth of the term $r_o^{2.5}$, the value of the term $h_o^{0.5}P/V_{soot}RT_o$ should be decreased appropriately. By adjusting the gap width h_o, helium pressure P, the rate of vapor generation $V_{soot}$and arc temperature $T_o$through deliberate variation of externally controlled parameters (electrodeFR, helium pressure, and arc current), this compensation may become possible. These adjustments were implemented with 25-mm diameter anodes of the same 3Co/Ni composition and resulted in a product that contained on the average ~15 wt% of SWNTs, which is nearly the same as the SWNT yield obtained with commonly used 8-mm diameter rods under optimal conditions. Experiments were done with the large-scale arc discharge apparatus. Clothlike soot with ~12 wt% SWNT yield can be peeled off the walls of the reactor chamber as hand towel–sized sheets. The average SWNT yield in the large collaret on the cathode deposit is ~25 wt%. The soot production rate with 25-mm-diameter rods makes ~100 g/h; thus a 20-fold scalingfactor for the process is attained compared with 8-mm diameter rods [26]. The process using 25-mm-diameter rods can be deemed semi-continuous, as loading a new rod takes a small fraction of the operation cycle. Moreover, in this sense the process can be rendered virtually continuous by arranging the automatic change of rods and continuous harvest of the soot, technical improvements that are already implemented at some laboratory scale arc installations. Finally, a further increase in rod diameter to 50 to 75 mm appears quite feasible and expedient.

IV. CONCLUSIONS

The mechanism of the SWNT synthesis in the arc discharge processes appears to be fairly simple. It is governed mainly by the dynamics of hot vapor cooling and carbon diffusion through the bulk metal catalyst particle. It allows deliberate control of the arc processes and is the basis for the successful scaling-up efforts of the arc process. Semi quantitative treatment of the arc processes is possible. It provides a basis for a detailed mathematical modeling of arc reactors, which is necessary in order to design practical processes for maximum productivity, yield, and quality of SWNTs.

Scaling up the arc discharge processes of SWNT, DWNT, and MWNT production is possible and is realized in practice on an industrial scale. A production rate of 100 g/h of the raw product of each kind of these nanotubes is achieved per industrial apparatus. The economically reasonable limit for scaling up is already reached, but the challenge to further increase selectivity and specific productivity of the arc processes remains active.

Synthesis of SWNTs by the arc-discharge method is actually a CVD process that transforms amorphous carbon into a SWNT bundle with an appropriately large metal catalyst particle and proceeds in concordance with the DP kinetic mechanism. Arc synthesis of DWNTs in hydrogen atmosphere is a CVD process that grows one DWNT from an equal-diameter catalytic metal particle, which uses thermally stable light hydrocarbons for the carbon source. The process obeys the regularities of the DP kinetic model. Tube-growth termination in the DP model can be attributed to a cold explosion in the thermally non-equilibrium catalytic particle.

Diffusion of carbon through the bulk metal catalyst particle is the rate-limiting step in all kinetically studied systems that grow long nanotubes. Therefore, in order to reach higher production rates, high-temperature processes should be developed, including CVD processes, ranging up to 1500°C, which appears to be the temperature limit for diffusion-controlled transition metal catalytic systems. For this development, the most difficult problem to resolve is to prevent thermal noncatalytic dehydrogenative condensation of the carbon source. In arc discharge synthesis of SWNTs, this problem is obviated by the use of amorphous carbon for the feedstock. Another important problem is the design of appropriate metal catalysts, which remains a poorly explored area.

A current fundamental and practical challenge is selective synthesis of TWNTs. It does not seem to be an insurmountable problem, as arc DWNT synthesis can produce small but variable amounts of TWNTs, depending on conditions. Study of TWNT occurrence and deliberate variation of arc-system parameters based on the quantitative knowledge of catalyst performance accumulated so far, however scarce, may lead to higher TWNT selectivity and eventually to desired domination of TWNTs in the products.

REFERENCES

[1.] N.A. Kiselev et al., Carbon 37, 1093 (1999).

[2.] S. Iijima, Nature 354, 56 (1991).

[3.] T.W. Ebbesen and P.M. Ajayan, Nature 358, 220 (1992).

[4.] T.W. Ebbesen et al., Chem. Phys. Lett. 209, 83 (1993).

[5.] D.T. Colbert et al., Science 266, 1218 (1994).
[6.] X.K. Wang et al., Carbon 33, 949 (1995).
[7.] S. Serapin et al., Carbon 31, 685 (1993).
[8.] Y. Saito et al., Chem. Phys. Lett. 204, 277 (1993).
[9.] P.M. Ajayan et al., J. Mater. Res. 12, 244 (1997).
[10.] G.H. Taylor et al., J. Cryst. Growth 135, 157 (1994).
[11.] A.S. Kotosonov and S.V. Kuvshinnikov, Phys. Lett. A 240, 377 (1997).
[12.] H. Ajiki and T. Ando, J. Phys. Soc. Jpn. 62, 2470 (1993).
[1.] R. Saito, G. Dresselhaus, and M. Dresselhaus, Phys. Rev. B 50, 14698 (1994).
[2.] V.I. Tsebro, O.E. Omel'yanovskii, and A.P. Moravskii, JETP Lett. 70, 462 (1999).
[3.] S. Frank et al., Science 280, 1744 (1998).
[4.] V.P. Bubnov et al., Russ. Chem. Bull. 43, 746 (1994).
[5.] A.S. Kotosonov, D.V.Shilo, and A.P. Moravskii, Phys. Sol. State 44, 666 (2002).
[6.] A. Huczko et al., J. Phys. Chem. A 101, 1267 (1997).
[7.] R.E. Smalley, Mater. Sci. Eng. B 19, 1 (1993).
[8.] J. Abrahamson, Carbon 12, 111 (1974).
[9.] J.M. Jones et al., Carbon 34, 231 (1996).
[10.] A.V. Krestinin and A.P. Moravsky, Chem. Phys. Lett. 286, 479 (1998).
[11.] E.G. Gamaly and T.W. Ebbesen, Phys. Rev. B 53, 2083 (1995).
[12.] T. Guo et al., J. Phys. Chem. 99, 10694 (1995).
[13.] A.A. Setlur et al., ECS Proceedings 98-8, 897 (1998).
[14.] R.O. Loutfy et al., in: Persp. Full. Nanotech., Ed. E. Osawa, Kluwer, Dordrecht, p. 35 (2002).
[15.] R.E. Smalley, Acc. Chem. Research 25, 98 (1992).
[16.] Y-K. Kwon et al., Phys. Rev. Lett. 79, 2065 (1997).
[17.] P.M. Ajayan, T. Ichihashi, and S. Iijima, Chem. Phys. Lett. 202, 384 (1993).
[18.] S. Iijima and T. Ichihashi, Nature 363, 603 (1993).
[19.] D. S. Bethune et al., Nature 363, 605 (1993).
[20.] P.M. Ajayan et al., Chem. Phys. Lett. 215, 509 (1993).
[21.] S. Serapin et al., Chem. Phys. Lett. 217, 191 (1994).
[22.] Serapin and D. Zhou, Appl. Phys. Lett. 64, 2087 (1994).
[23.] C.H. Kiang et al., J. Phys. Chem. 98, 6612 (1994).
[24.] J.M. Lambert et al., Chem. Phys. Lett. 226, 364 (1994).
[25.] X. Lin et al., Appl. Phys. Lett. 64, 181 (1994).
[26.] P.M. Ajayan et al., Phys. Rev. Lett. 72, 1722 (1994).
[27.] C. Guerret-Piecourt et al., Nature 372, 761 (1994).
[28.] C.H. Kiang et al., Carbon 33, 903 (1995)
[29.] Y. Saito, K. Kawabata, and M. Okuda, J. Phys. Chem. 99, 16076 (1995).

[30.] J.M. Lambert, P.M. Ajayan, and P. Bernier, Synth. Met. 70, 1475 (1995).
[31.] M. Ata et al., J. Appl. Phys. 34, 4207 (1995).
[32.] W.K. Maser et al., Synth. Met. 81, 243 (1996).
[33.] A. Loiseau and H. Pascard, Chem. Phys. Lett. 256, 246 (1996).
[34.] C. Journet et al., Nature 388, 756 (1997).
[35.] C. Journet and P. Bernier, Appl. Phys. A67, 1 (1998).
[36.] M. Yudasaka et al., Chem. Phys. Lett. 312, 155 (1999).
[37.] J. Gavillet et al., Carbon 40, 1649 (2002).
[38.] M.E. Itkis et al., Nano Lett. 3, 309 (2003).
[39.] R.O. Loutfy et al., IWFAC'99, Abstracts, St. Petersburg, 109 (1999).
[40.] D. Golberg et al., Carbon 38, 2017 (2000).
[41.] M. Takizawa et al., Chem. Phys. Lett. 302, 146 (1999).
[42.] S. Bandow et al., Phys. Rev. Lett. 80, 3779 (1998).
[43.] M. Lami de la Chapelle et al., AIP Conf. Proc. 486: Ed. H. Kuzmany et al., 292 (1999).
[44.] S. Farhat et al., J. Chem. Phys. 115, 6752 (2001).
[45.] M. Takizawa et al., Chem. Phys. Lett. 326, 351, (2000).
[46.] A.C. Dillon et al., Chem. Phys. Lett. 316, 13, (2000).
[47.] I. Hinkov et al., Proc. 6th ADC/2nd FCT Joint Conf., 816 (2001).
[48.] A. Thess et al., Science 273, 483 (1996).
[49.] R.O. Loutfy et al., IWFAC'99, Abstracts, St. Petersburg, 117 (1999).
[50.] A.V. Krestinin and A.P. Moravsky, Chem. Phys. Reports 18, 3 (1999).
[51.] G.N. Abramovich, Applied Gas Dynamics, Nauka, Moscow (1969).
[52.] A.P. Moravsky et al., Fullerene Sci. Tech. 6, 453 (1998).
[53.] B.I. Yakobson and R.E. Smalley, Am. Scientist 85, 324 (1997).
[54.] R.T.K. Baker et al., J. Catal. 30, 86 (1973).
[55.] A. Oberlin, M. Endo, and T. Koyama, J. Cryst. Growth 32, 335 (1976).
[56.] G.G. Tibbets, J. Cryst. Growth 66, 632 (1984).
[57.] R.T.K. Baker and J.J. Chludzinski, J. Phys. Chem. 90, 4 (1986).
[58.] Y. Saito et al., Jpn. J. Appl. Phys. 33, 526 (1994).
[59.] Y. Saito, Carbon 33, 979 (1995).
[60.] A. Maiti, C.J. Brabec, and J. Bernholc, Phys. Rev. B Rapid Commun. 55, 6097 (1997).
[61.] J. Lefebvre, R. Antonov, and A.T. Johnson, Appl. Phys. A 67, 71 (1998).
[62.] H. Kanzow and A. Ding, Phys. Rev. B 60, 11180 (1999).
[63.] A. Gorbunov et al., Carbon 40, 113 (2002).
[64.] H. Kataura et al., Carbon 38, 1691 (2000).
[65.] O.P. Krivoruchko and V.I. Zaikovskii, Mendeleev Commun. 3, 97 (1998).
[66.] V. Zait, Diffusion in Metals, Nauka, Moscow, 1958.

ISBN: 978-93-86171-76-4

[67.] J.M. Cowley et al., Chem. Phys. Lett. 265, 379 (1997).
[68.] A. Hassanien et al., Appl. Phys. Lett. 73, 3839 (1998).
[69.] S. Rols et al., Eur. Phys. J. B 10, 263 (1999).
[70.] J.W.G. Wildoer et al., Nature 391, 59 (1998).
[71.] T.W. Odom et al., Nature 391, 62 (1998).
[72.] D. Golberg et al., Carbon 37, 1858 (2000).
[73.] G. van Tendeloo et al., Carbon 36, 487 (1998).
[74.] J. Kurti et al., AIP Conf. CP486 Ext. Abstr., Ed. H. Kuzmany et al., 278 (1999).
[75.] S. Eisebitt et al., AIP Conf. CP486 Ext. Abstr., Ed. H. Kuzmany et al., 304 (1999).
[76.] W. Clauss et al., AIP Conf. CP486 Ext. Abstr., Ed. H. Kuzmany et al., 308 (1999).
[77.] J. Hutchison et al., Carbon 39, 761 (2001).
[78.] J.M. Zuo et al., Science 300, 1419 (2003).
[79.] A.P. Moravsky et al., unpublished results.
[80.] A.P. Moravsky and R.O. Loutfy, US Patent pending (2000).
[81.] L.J. Ci et al., Chem. Phys. Lett. 359, 63 (2002).
[82.] W.C. Ren et al., Chem. Phys. Lett. 359, 196 (2002).